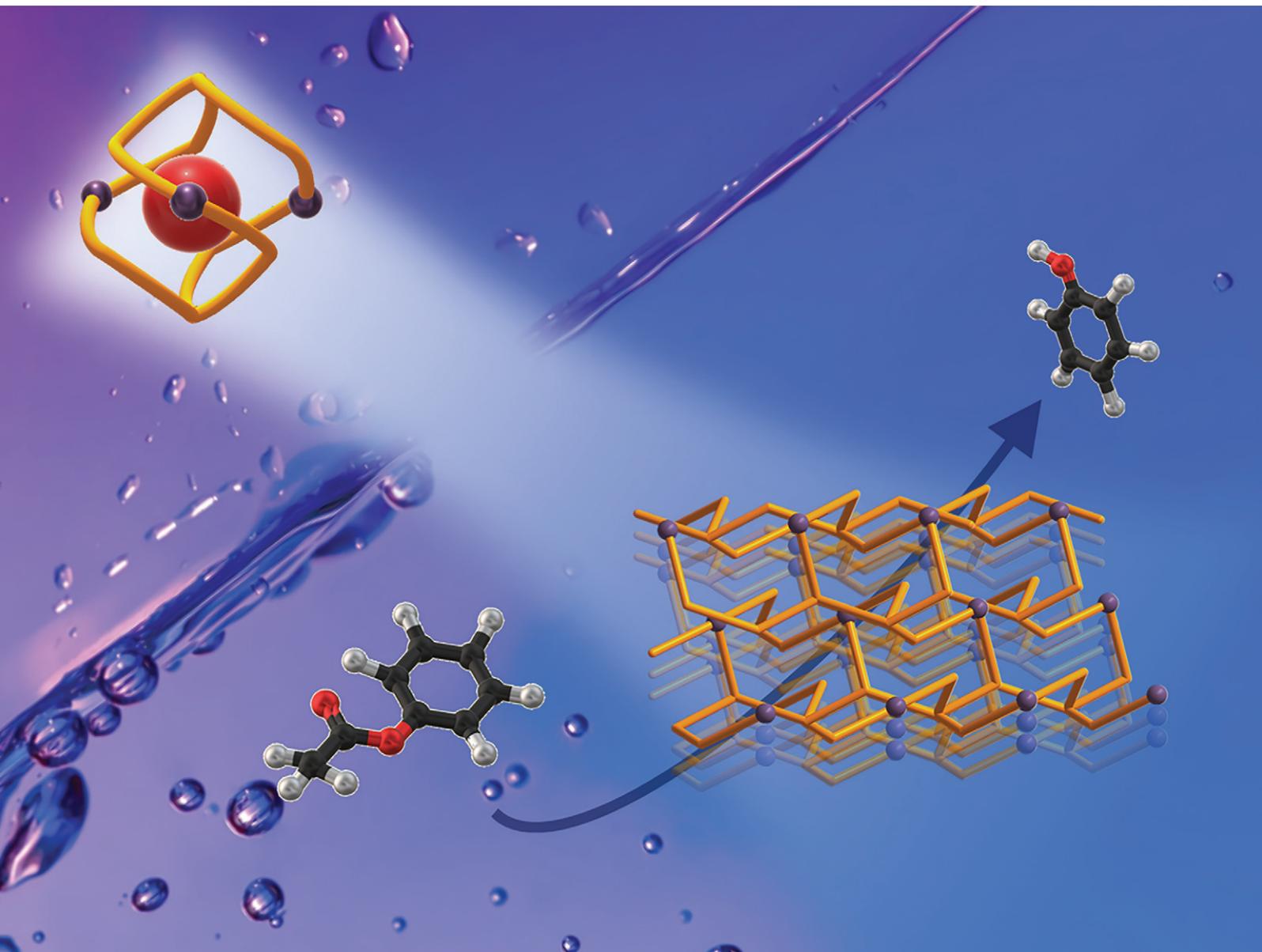# CrystEngComm

ROYAL SOCIETY
OF CHEMISTRY

PAPER
Ok-Sang Jung *et al.*
Construction and catalytic effects of solvent- and
metal(II)-dependent products: the process of
transformation of 0D structures into 3D structures

Construction and catalytic effects of solvent- and metal(II)-dependent products: the process of transformation of 0D structures into 3D structures†

Gyeongmin Kim, Jihun Han, Dongwon Kim and Ok-Sang Jung (ID) *

Self-assembly of Zn(NO$_3$)$_2$ with tris(2-(isoquinolin-5-yloxy)ethyl)amine (L) as a C_3-symmetric tridentate N-donor in a mixture of dioxane and acetonitrile gives rise to [NO$_3$@Zn$_3$(NO$_3$)$_5$L$_2$]·2CH$_3$CN in the form of crystals of sandwich-shaped cages encapsulating a nitrate, whereas the same self-assembly reaction in a different mixture, benzene and ethanol, produces [Zn(NO$_3$)L(H$_2$O)]NO$_3$·H$_2$O in the form of crystals of 3D networks with *cml* {4,6^2}$_2$\{4^2,6^{10},8^3\} topology. The most interesting feature is the transformation of [NO$_3$@Zn$_3$(NO$_3$)$_5$L$_2$]·2CH$_3$CN crystals into [Zn(NO$_3$)L(H$_2$O)]NO$_3$·H$_2$O crystals in ethanol. A significant difference in heterogeneous transesterification catalysis between the two species is observed. On the other hand, self-assembly of Co(NO$_3$)$_2$ with L gives rise to 3D networks, [Co(NO$_3$)L(H$_2$O)]NO$_3$·H$_2$O, whereas self-assembly of Ni(NO$_3$)$_2$ and Cu(NO$_3$)$_2$ with L produces sandwich-type cages, [NO$_3$@Ni$_3$(NO$_3$)$_3$L$_2$(H$_2$O)$_6$]2NO$_3$·C$_2$H$_5$OH·C$_6$H$_6$ and [NO$_3$@Cu$_3$(NO$_3$)$_5$L$_2$(C$_2$H$_5$OH)]·C$_2$H$_5$OH·2C$_6$H$_6$, respectively, with the latter notably showing heterogeneous catechol oxidation catalytic effects.

Introduction

Construction of diverse coordination architectures *via* combinations of metal cations and spacer donors and its geometric principle have beckoned chemists over the past decade,[1–10] especially after the discovery of practical task-specific functions. If the coordination components of metal cations and spacer donors could be desirably assembled, what would both the resultant structures and the applications of their assembled products be? Discovery of a methodology for synthesis of various coordination architectures *via* deliberate driving forces is a significant challenge, and not concomitantly, is also an intriguing idea in the area of coordination materials.[11–18] A prerequisite to the development of diverse coordination materials is the comprehension of the substantial driving forces behind the formation of different coordination networks for the same components. Furthermore, the process of interconversion between two different coordination assemblies from the same

components is a fascinating research topic relevant to developments in efficient adsorption/desorption, molecular recognition, anion exchange, and catalysis.[19–24] Thus, rich data on the geometry of metal cations with the binding sites, lengths, and flexibility of multidentate donors in mixture solvent systems might afford new avenues to efficient coordination materials. Indeed, the combination of first-row transition metal cations and flexible multidentate N-donors suggests such a route.[25] In this context, the two ambitious aims of the present article were to explore the transformation process between two different coordination species *via* both photoluminescence (PL) spectra and time-dependent morphology change, and to investigate the solvent and metal cation effects on the self-assembly of first-row transition M^{2+} cations with a new flexible tridentate donor. Additionally, heterogeneous catalysis reactions using the present coordination species, namely zinc(II) and copper(II), were attempted. These coordination species have been known to be useful in the transesterification of a wide range of esters with alcohols and the oxidation of various alcohols, respectively. In particular, zinc(II) species have been investigated and deemed to be useful metal cations for Lewis acids, metallo-enzymes, zinc finger proteins, and PL materials.[26–31]

Experimental

Reagents and measurement

All of the chemicals including M(NO$_3$)$_2$ (M(II) = Zn(II), Co(II), Ni(II), and Cu(II)) were purchased from Aldrich and used

Department of Chemistry, Pusan National University, Busan 46241, Republic of Korea. E-mail: oksjung@pusan.ac.kr; Fax: +82 51 5163522; Tel: +82 51 5103240

without further purification. ^{1}H NMR spectra were recorded on a Varian Mercury Plus 400 instrument operating at 400 MHz. Infrared spectra were obtained on a Nicolet 380 FT-IR spectrophotometer with samples prepared as KBr pellets. Elemental microanalyses (C, H, N) were performed on solid samples at the Pusan Center, KBSI, using a Vario-EL III. Thermal analyses were carried out under a dinitrogen atmosphere at a scan rate of 10 °C min^{-1} using a Labsys TGA-DSC 1600. Excitation and emission spectra were recorded on a Hitachi F-7000 spectrofluorometer.

Synthesis of tris(2-(isoquinolin-5-yloxy)ethyl)amine

Triethanolamine (3.96 mL, 30.0 mmol) was slowly added to a solution of stirred thionyl chloride (4.4 mL, 60.0 mmol) in chloroform (20 mL), and the mixture was further stirred at 25 °C for 1 h. Evaporation of the chloroform solution afforded a white solid, tris(2-chloroethyl)amine, in a 99.4% yield (6.1 g). The dried tris(2-chloroethyl)amine (2.4 g, 10.0 mmol) was slowly added to a mixture of 5-hydroxyisoquinoline (4.8 g, 33.3 mmol) and sodium hydroxide (2.0 g, 50.0 mmol) in ethanol (100.0 mL), and the reactant mixture was refluxed at 80 °C for 8 h. Evaporation of the ethanol solution afforded a red liquid. Then, the chloroform solution of the liquid product was washed with aqueous NaOH solution several times, and the chloroform layer was dried over anhydrous sodium sulfate. The pink solid obtained by evaporation of chloroform was purified by column chromatography on silica gel (dichloromethane : ethyl acetate : hexane = 80 : 15 : 5 volumes as eluent) to obtain the product in a 76.0% yield. m. p. 150 °C (dec.). Anal. Calcd. for C$_{33}$H$_{30}$N$_4$O$_3$: C, 74.70; H, 5.70; N, 10.56%. Found: C, 74.40; H, 5.52; N, 10.28%. IR (KBr pellet, cm^{-1}): 3055(w), 2925(m), 2866(w), 1628(w), 1582(s), 1492(s), 1458(m), 1438(s), 1393(s), 1365(s), 1323(s), 1278(s), 1255(s), 1217(m), 1178(m), 1117(m), 1062(m), 1020(m), 943(w), 916(m), 829(s), 803(m), 750(s), 649(w), 580(w), 446(w), 408(w). ^{1}H NMR (in Me$_2$SO-d_6, δ): 9.20 (s, 3H), 8.10 (d, J = 5.75 Hz, 3H), 7.79 (d, J = 5.88 Hz, 3H), 7.60 (d, J = 8.25 Hz, 6H), 7.53 (t, J = 7.94 Hz, 3H), 7.20 (d, J = 7.63 Hz, 3H), 4.36 (t, J = 5.31 Hz, 6H), 3.34 (t, J = 5.38 Hz, 6H).

[Zn(NO$_3$)L(H$_2$O)]NO$_3$·H$_2$O

An ethanol solution (4.0 mL) of zinc(II) nitrate hexahydrate (3.6 mg, 0.012 mmol) was carefully layered onto a benzene solution (4.0 mL) of L (6.4 mg, 0.012 mmol). After 3 days, colorless crystals suitable for single crystal X-ray crystallography were obtained in an 85% yield. m.p. 218 °C (dec.). Anal. Calcd. for C$_{33}$H$_{34}$ZnN$_6$O$_{14}$: C, 49.30; H, 4.26; N, 10.45%. Found: C, 48.90; H, 4.30; N, 11.10%. IR (KBr pellet, cm^{-1}): 3065(w), 2945(w), 2817(w), 1631(w), 1595(m), 1499(s), 1445(m), 1441(m), 1384(s), 1280(s), 1255(m), 1221(m), 1185(m), 1117(m), 1069(w), 1041(m), 927(m), 837(m), 809(m), 751(m), 644(w), 584(w), 545(w), 473(w), 415(w). ^{1}H NMR (dissociated in Me$_2$SO-d_6, δ): 9.20 (s, 3H), 8.10 (d, J = 5.75 Hz, 3H), 7.79 (d, J = 5.88 Hz, 3H), 7.60 (d, J = 8.25 Hz, 6H), 7.53 (t, J = 7.94 Hz, 3H), 7.20 (d, J = 7.63 Hz, 3H), 4.36 (t, J = 5.31 Hz, 6H), 3.34 (t, J = 5.38 Hz, 6H).

[NO$_3$@Zn$_3$(NO$_3$)$_5$L$_2$]·2CH$_3$CN

An acetonitrile solution (4.0 mL) of zinc(II) nitrate hexahydrate (3.6 mg, 0.012 mmol) was carefully layered onto a dioxane solution (4.0 mL) of L (6.4 mg, 0.012 mmol). After 4 days, colorless crystals suitable for single crystal X-ray crystallography were obtained in an 84% yield. m.p. 150 °C (dec.). Anal. Calcd. For C$_{70}$H$_{66}$Zn$_3$N$_{16}$O$_{24}$: C, 49.12; H, 3.89; N, 13.09%. Found: C, 49.20; H, 3.71; N, 13.10%. IR (KBr pellet, cm^{-1}): 3055(w), 2964(m), 2930(w), 1628(w), 1600(m), 1497(s), 1464(m), 1443(m), 1382(s), 1283(s), 1255(m), 1185(m), 1121(m), 1079(w), 1044(m), 929(m), 833(m), 803(m), 759(m), 646(w), 582(w), 540(w), 479(w), 418(w). ^{1}H NMR (dissociated in Me$_2$SO-d_6, δ): 9.20 (s, 3H), 8.10 (d, J = 5.75 Hz, 3H), 7.79 (d, J = 5.88 Hz, 3H), 7.60 (d, J = 8.25 Hz, 6H), 7.53 (t, J = 7.94 Hz, 3H), 7.20 (d, J = 7.63 Hz, 3H), 4.36 (t, J = 5.31 Hz, 6H), 3.34 (t, J = 5.38 Hz, 6H).

[Co(NO$_3$)L(H$_2$O)]NO$_3$·H$_2$O

An ethanol solution (4.0 mL) of cobalt(II) nitrate hexahydrate (3.5 mg, 0.012 mmol) was carefully layered onto a benzene solution (4.0 mL) of L (6.4 mg, 0.012 mmol). After 2 days, white crystals suitable for single crystal X-ray crystallography were obtained in a 92% yield. m.p. 225 °C (dec.). Anal. Calcd. for C$_{33}$H$_{34}$CoN$_6$O$_{14}$: C, 49.69; H, 4.30; N, 10.54%. Found: C, 46.40; H, 4.32; N, 10.60%. IR (KBr pellet, cm^{-1}): 3444(s), 2947(w), 2813(w), 1633(m), 1598(s), 1499(m), 1475(m), 1439(m), 1387(s), 1326(w), 1285(s), 1259(w), 1211(w), 1181(w), 1116(m), 1042(m), 922(w), 833(m), 809(m), 747(m), 650(w), 547(w), 484(w). ^{1}H NMR (dissociated in Me$_2$SO-d_6, δ): 9.20 (s, 3H), 8.10 (d, J = 5.75 Hz, 3H), 7.79 (d, J = 5.88 Hz, 3H), 7.60 (d, J = 8.25 Hz, 6H), 7.53 (t, J = 7.94 Hz, 3H), 7.20 (d, J = 7.63 Hz, 3H), 4.36 (t, J = 5.31 Hz, 6H), 3.34 (t, J = 5.38 Hz, 6H).

[NO$_3$@Ni$_3$(NO$_3$)$_3$L$_2$(H$_2$O)$_6$]2NO$_3$·C$_2$H$_5$OH·C$_6$H$_6$

An ethanol solution (4.0 mL) of nickel(II) nitrate hexahydrate (3.5 mg, 0.012 mmol) was carefully layered onto a benzene solution (4.0 mL) of L (6.4 mg, 0.012 mmol). After 2 days, white crystals suitable for single crystal X-ray crystallography were obtained in a 78% yield. m.p. 235 °C (dec.). Anal. Calcd. for C$_{74}$H$_{84}$Ni$_3$N$_{14}$O$_{31}$: C, 48.26; H, 4.60; N, 10.65%. Found: C, 48.10; H, 4.15; N, 10.20%. IR (KBr pellet, cm^{-1}): 3385(s), 2944(w), 2814(w), 1631(m), 1599(m), 1498(m), 1476(m), 1441(m), 1383(s), 1327(m), 1280(s), 1254(m), 1222(w), 1182(w), 1116(m), 1037(m), 1022(w), 922(w), 838(w), 808(w), 746(m), 6654(w), 535(w). ^{1}H NMR (dissociated in Me$_2$SO-d_6, δ): 9.20 (s, 3H), 8.10 (d, J = 5.75 Hz, 3H), 7.79 (d, J = 5.88 Hz, 3H), 7.60 (d, J = 8.25 Hz, 6H), 7.53 (t, J = 7.94 Hz, 3H), 7.20 (d, J = 7.63 Hz, 3H), 4.36 (t, J = 5.31 Hz, 6H), 3.34 (t, J = 5.38 Hz, 6H).

$[NO_3@Cu_3(NO_3)_5L_2(C_2H_5OH)]·C_2H_5OH·2C_6H_6$

An ethanol solution (4.0 mL) of copper(II) nitrate hexahydrate (3.5 mg, 0.012 mmol) was carefully layered onto a benzene solution (4.0 mL) of L (6.4 mg, 0.012 mmol). After 7 days, blue crystals suitable for single crystal X-ray crystallography were obtained in an 88% yield. m.p. 239 °C (dec.). Anal. Calcd. for $C_{82}H_{84}Cu_3N_{14}O_{26}$: C, 52.60; H, 4.52; N, 10.48%. Found: C, 51.90; H, 4.48; N, 10.23%. IR (KBr pellet, cm^{-1}): 3485(s), 2379(w), 2344(w), 1650(m), 1595(m), 1390(s), 1286(w), 1187(w), 1120(w), 1051(w), 841(w), 757(w), 650(w), 531(w).

Transformation of $[NO_3@Zn_3(NO_3)_5L_2]·2CH_3CN$ into $[Zn(NO_3)L(H_2O)]NO_3·H_2O$

Single crystals of $[NO_3@Zn_3(NO_3)_5L_2]·2CH_3CN$ (0.003 mmol) left in 1.5 mL of 95% ethanol resulted in the formation of $[Zn(NO_3)L(H_2O)]NO_3·H_2O$ in a 70% yield (based on Zn(II)) after 1 day.

Transesterification catalysis

The zinc(II) catalysts were employed as catalysts for the transesterification reaction of phenyl acetate with methanol. Each zinc(II) catalyst (80, 172 mg, 0.1 mmol) and phenyl acetate (0.13 mL, 1.0 mmol) were stirred in methanol (10 mL), and heated up to 40 °C. The catalytic process was monitored by referring to the ^1H NMR spectra.

Catechol oxidation catalysis

3,5-Di-*tert*-butylcatechol (3,5-DBuCat) was employed as the substrate for catalytic oxidation reactions. The present copper(II) catalysts (18.7 mg, 0.01 mmol) were treated with the substrate (22.3 mg, 0.1 mmol) in acetone (10 mL) at 40 °C under aerobic conditions. The catalytic yields were monitored by referring to the UV-vis and ^1H NMR spectra.

Single crystal X-ray crystallography

All of the X-ray diffraction data (except for $[NO_3@Cu_3(NO_3)_5L_2(C_2H_5OH)]·C_2H_5OH·2C_6H_6$) were measured at 153 K or 223 K with synchrotron radiation (λ = 0.63000–0.70000 Å) on a Rayonix MX225HS detector at 2D SMC with a silicon (111) double-crystal monochromator (DCM) at the Pohang Accelerator Laboratory, Korea. The PAL BL2D-SMDC program[32] was used for data collection (detector distance: 66 mm, omega scan: $\Delta\omega$ = 3°, exposure time: 1 s per frame), and HKL3000sm (ver. 703r)[33] was used for cell refinement, reduction, and absorption correction. X-ray data on $[NO_3@Cu_3(NO_3)_5L_2(C_2H_5OH)]·C_2H_5OH·2C_6H_6$ were collected on a Bruker SMART automatic diffractometer with graphite-monochromated Mo Kα radiation (λ = 0.71073 Å). Thirty-six (36) frames of 2D diffraction images were collected and processed to obtain the cell parameters and orientation matrix. The data were corrected for Lorentz and polarization effects. The absorption effects were corrected using the multi-scan method (SADABS).[34] The structures were solved using the direct method (SHELXS) and refined by a full-

matrix least squares technique (SHELXL 2018/3).[35] The non-hydrogen atoms were refined anisotropically, and the hydrogen atoms were placed in calculated positions and refined only for the isotropic thermal factors. For only $[NO_3@Ni_3(NO_3)_3L_2(H_2O)_6]2NO_3·C_2H_5OH·C_6H_6$, two nitrates, one ethanol and one benzene solvate were squeezed by using the SQUEEZE routine in PLATON.[36] The crystal parameters and procedural information corresponding to the data collection and structure refinement are listed in Tables S1 and S2.†

Results and discussion

Synthesis

The new flexible tridentate ligand, tris(2-(isoquinolin-5-yloxy)ethyl)amine (L), was synthesized by the reaction of tris(2-chloroethyl)amine with 5-hydroxyisoquinoline in a high yield. As shown in Scheme 1, the self-assembly of $Zn(NO_3)_2$ in acetonitrile with L in dioxane produced colorless crystals consisting of discrete cages encapsulating a nitrate, $[NO_3@Zn_3(NO_3)_5L_2]·2CH_3CN$, whereas the self-assembly in a different mixture of ethanol and benzene afforded crystals of 3D networks, $[Zn(NO_3)L(H_2O)]NO_3·H_2O$. This result confirmed the self-assembly reactions to have been strongly dependent on the reaction solvents. Moreover, the crystals consisting of cages, $[NO_3@Zn_3(NO_3)_5L_2]·2CH_3CN$, were left in ethanol, and transformed into $[Zn(NO_3)L(H_2O)]NO_3·H_2O$ in the form of crystals of 3D networks after 1 day. On the other hand, the self-assembly of $Co(NO_3)_2$ with L gave rise to $[Co(NO_3)L(H_2O)]NO_3·H_2O$ in the form of crystals of 3D networks, whereas the self-assembly reactions of $Ni(NO_3)_2$ and $Cu(NO_3)_2$ with L in the same solvent mixture produced $[NO_3@Ni_3(NO_3)_3L_2(H_2O)_6]2NO_3·C_2H_5OH·C_6H_6$ and $[NO_3@Cu_3(NO_3)_5L_2(C_2H_5OH)]·C_2H_5OH·2C_6H_6$, respectively, in the form of discrete cages, indicating that such self-assembly reactions exhibit metal(II) ion effects. The self-assembly reactions were originally carried out at the mole ratio of 1:1, but the formation of the products was not significantly affected by the change of the reactant mole ratio or concentration. All of the species are insoluble in water, chloroform, acetone, and dichloromethane, but are easily dissociated in polar organic solvents such as dimethyl sulfoxide and *N,N*-dimethylformamide. $[NO_3@Zn_3(NO_3)_5L_2]·2CH_3CN$ is slowly dissociated in ethanol. The compositions and structures of all of the products were confirmed by elemental analyses, ^1H NMR (Fig. S1†), IR (Fig. S2†), thermal analysis (Fig. S3†), and single crystal X-ray diffraction. Thermogravimetric analysis indicated that $[NO_3@Zn_3(NO_3)_5L_2]·2CH_3CN$ and $[Zn(NO_3)L(H_2O)]NO_3·H_2O$ were stable up to 260 and 270 °C, respectively. Their solvate acetonitrile molecules and water molecules were evaporated at 145–180 and 50–80 °C, respectively.
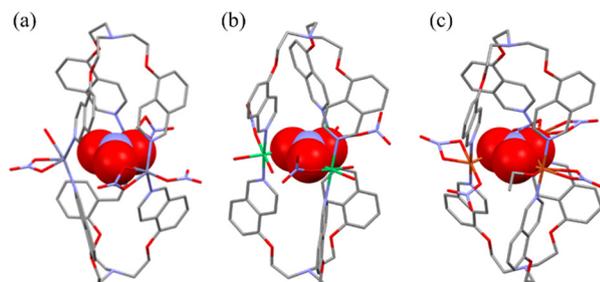
Crystal structures

The X-ray single-crystal characterization provided discrete cages or 3D networks depending on the solvents and
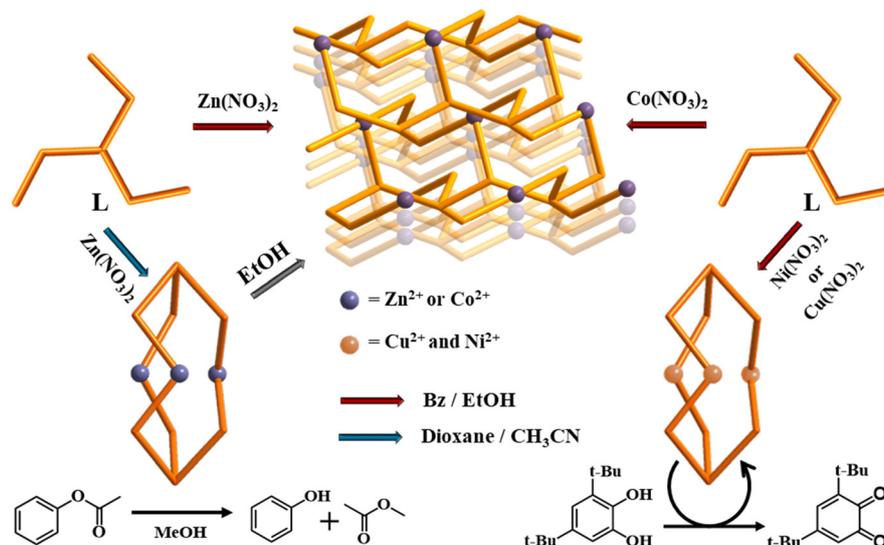
Scheme 1 Overall synthesis including dimensional transformation and catalysis of M₃L₂ cages into 3D networks.

transition metal(ɪɪ) cations (Scheme 1 and Fig. 1 and 2), and the relevant bond distances and angles are listed in Table 1. For [NO₃@Zn₃(NO₃)₅L₂]·2CH₃CN, L is connected to three Zn(ɪɪ) ions (Zn–N = 2.001(4)–2.054(3) Å) in a tridentate fashion to form a discrete sandwich-type Zn₃L₂ cage with a Zn···Zn separation of 5.258(2)–5.887(1) Å. The local geometries around the three zinc(ɪɪ) ions correspond to three different six-to-seven coordination arrangements with two N donors from two Ls and four-to-five O donors from nitrate anions (Zn–O = 1.999(7)–2.071(7) Å). One nitrate is encapsulated inside the cage and interacts with three Zn(ɪɪ) ions. Acetonitrile solvates are positioned in the vacancy of the inter-cage. The shortest inter-cage distance is O(NO₃) ···O(NO₃) = 3.108(2) Å (see the structure (Fig. S4†) packed in *abab*… along the *a*-axis). The crystal structures of [NO₃@Ni₃(NO₃)₃L₂(H₂O)₆]2NO₃·C₂H₅OH·C₆H₆ and [NO₃@Cu₃(NO₃)₅L₂(C₂H₅OH)]·C₂H₅OH·2C₆H₆ are basically the same cage, though with a slightly different coordination geometry around each central metal cation. For each crystal, solvate molecules are positioned in the vacancy of

the inter-cages without any significant interactions. In contrast, the crystal structure of [Zn(NO₃)L(H₂O)]NO₃·H₂O shows that L is coordinated to three Zn(ɪɪ) ions in a tridentate mode to produce a 3D network with *cml* {4,6²}₂{4²,6¹⁰,8³} topology, as depicted in Fig. 2 using the known program.[37] The geometry around the Zn(ɪɪ) cation is an octahedral arrangement with three N donors from three Ls and one bidentate nitrate and one water molecule. Both a nitrate counteranion and a water solvate molecule occupy the vacancy of the networks. The crystal structure of [Co(NO₃)L(H₂O)]NO₃·H₂O is the same 3D network. The conformations of L in the cages and the 3D networks are quite different: the L moiety of the cages and the 3D networks is in a tripodal and a triaxial fashion, respectively (Fig. S5†).

Fig. 1 Crystal structures of [NO₃@Zn₃(NO₃)₅L₂]·2CH₃CN (a), [NO₃@Ni₃(NO₃)₃L₂(H₂O)₆]2NO₃·C₂H₅OH·C₆H₆ (b), and [NO₃@Cu₃(NO₃)₅L₂(C₂H₅OH)]·C₂H₅OH·2C₆H₆ (c). The encapsulated nitrate anion is depicted in a space-filling mode: C (gray), O (red), N (sky blue), Zn (dark blue), Ni (green), and Cu (orange).
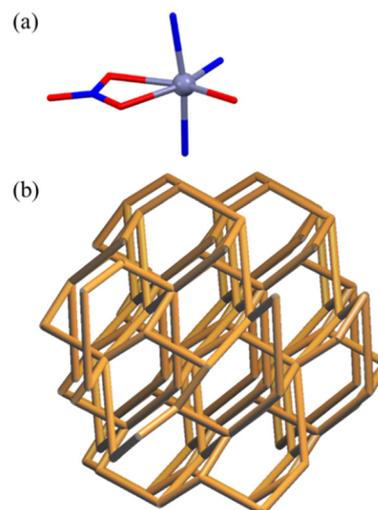
Fig. 2 Local geometry around M²⁺ (a) and 3D networks of [Zn(NO₃)L(H₂O)]NO₃·H₂O and [Co(NO₃)L(H₂O)]NO₃·H₂O with *cml* {4,6²}₂{4²,6¹⁰,8³} topology (b).

Table 1 Relevant distances (Å) and angles (°) for the five crystal structures

	$[NO_3@Zn_3(NO_3)_5L_2]\cdot 2CH_3CN$	$[NO_3@Ni_3(NO_3)_3L_2(H_2O)_6]2NO_3\cdot C_2H_5OH\cdot C_6H_6$	$[NO_3@Cu_3(NO_3)_5L_2(C_2H_5OH)]\cdot C_2H_5OH\cdot 2C_6H_6$
M–N (quinoline) (Å)	2.001(4)–2.054(3)	2.11(1)–2.131(4)	1.992(7)–2.024(8)
M–O (anion) (Å)	1.999(7)–2.071(7)	2.036(8)–2.16(1)	1.98(2)–2.256(9)
M⋯M (Å)	5.258(2)–5.887(1)	5.1759(8)	4.7543(4)–5.6949(5)
N–M–N (°)	120.5(2)–128.5(2)	177.3(3)	167.6(4)–178.3(3)

|	$[Zn(NO_3)L(H_2O)](NO_3)\cdot H_2O$	$[Co(NO_3)L(H_2O)](NO_3)\cdot H_2O$
M–N (quinoline) (Å)	2.091(3)–2.179(3)	2.103(3)–2.175(3)
M–O (anion) (Å)	2.206(3)	2.197(3)
M–O (H₂O) (Å)	2.031(3)	2.056(3)

Construction principle and transformation

Self-assembly of first-row transition metal(II) cations with the new flexible tridentate ligand, tris(2-(isoquinolin-5-yloxy) ethyl)amine (L), can principally construct 0D, 1D, 2D, and 3D coordination architectures. And in fact, in the present case, the self-assembly of $Zn(NO_3)_2$ with L afforded 0D cages and 3D networks depending on the solvents employed. In the polar solvent system of dioxane and acetonitrile, self-assembly gave rise to a discrete cage, Zn_3L_2, with an encapsulated nitrate anion, whereas in the mixture of benzene and ethanol, it produced 3D networks with *cml* $\{4,6^2\}_2\{4^2,6^{10},8^3\}$ topology, owing presumably to the solvation energy and solubility difference in the self-assembly of the d^{10} Zn(II) cation with the flexible tridentate L. That is, the flexible conformation of L can contribute to the formation of solvent-dependent structures. In particular, when the single crystals of $[NO_3@Zn_3(NO_3)_5L_2]\cdot 2CH_3CN$ were immersed in ethanol, they were slowly dissociated. Thus, the original crystals began to slowly transform to form new thermodynamic crystals of $[Zn(NO_3)L(H_2O)]NO_3\cdot H_2O$ in 95% ethanol (Fig. 3). This is an unusual observation, in which the original crystals transformed easily into new and stable crystals, depending on the solvents. Upon the measurement of the solid photoluminescence (PL) spectra (λ_{ex} = 315 nm) of the two present zinc(II) species $[NO_3@Zn_3(NO_3)_5L_2]\cdot 2CH_3CN$ and $[Zn(NO_3)L(H_2O)]NO_3\cdot H_2O$, together with those of L, the

PL peaks of $[NO_3@Zn_3(NO_3)_5L_2]\cdot 2CH_3CN$ (λ_{max} = 435 nm) and $[Zn(NO_3)L(H_2O)]NO_3\cdot H_2O$ (λ_{max} = 405 and 470 nm) were red-shifted relative to the corresponding L (λ_{max} = 370 nm) (Fig. 4). The ligand's intrinsic characteristics play a pivotal role in the PL appearance of the two zinc(II) species. Indeed, these results suggest that the complexes' emission bands can be ascribed to the ligand-to-metal charge transfer (LMCT).[38,39] Moreover, the transformation process of $[NO_3@Zn_3(NO_3)_5L_2]\cdot 2CH_3CN$ into $[Zn(NO_3)L(H_2O)]NO_3\cdot H_2O$ could be confirmed by the PL spectra, as depicted in the figure: that is, when a drop of ethanol was placed on the crystals of $[NO_3@Zn_3(NO_3)_5L_2]\cdot 2CH_3CN$, the PL spectral change was in agreement with the aforementioned original solid PL spectrum of $[Zn(NO_3)L(H_2O)]NO_3\cdot H_2O$. Formation of such solvent-dependent structures can be ascribed to both the d^{10} metal(II) cation (see the Irving–Williams series)[40] and the flexible tridentate L. The present self-assembly of $Co(NO_3)_2$ with L in a mixture of ethanol and benzene yielded the same 3D network, whereas that of $Ni(NO_3)_2$ and $Cu(NO_3)_2$ with L in the same solvent produced an M_3L_2 cage encapsulating a nitrate. That is, the two products are dependent on the M^{2+} cation. Thus, for Co(II), Ni(II), and
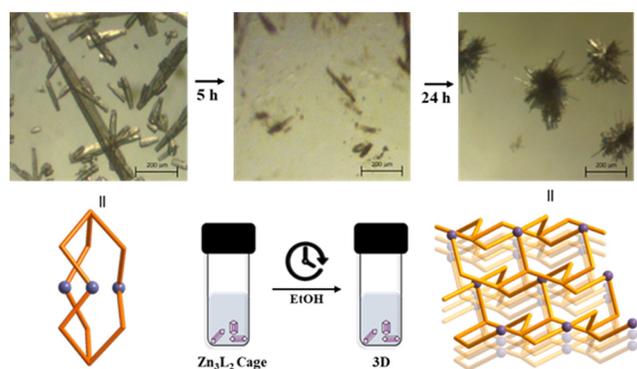
Fig. 3 Transformation process including morphology change of $[NO_3@Zn_3(NO_3)_5L_2]\cdot 2CH_3CN$ into $[Zn(NO_3)L(H_2O)]NO_3\cdot H_2O$ in 95% ethanol.
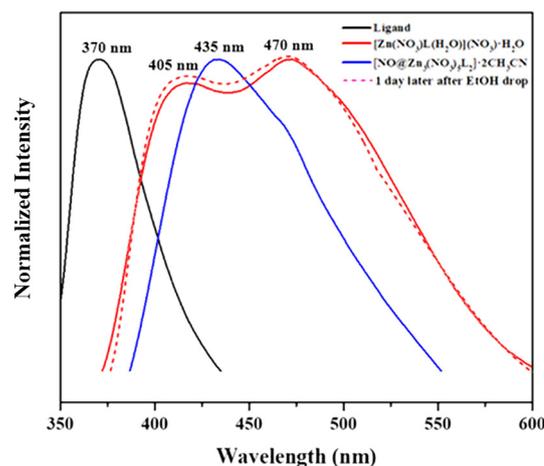
Fig. 4 PL spectra of L (black), $[NO_3@Zn_3(NO_3)_5L_2]\cdot 2CH_3CN$ (blue), and $[Zn(NO_3)L(H_2O)]NO_3\cdot H_2O$ (red), and transformation of $[NO_3@Zn_3(NO_3)_5L_2]\cdot 2CH_3CN$ into $[Zn(NO_3)L(H_2O)]NO_3\cdot H_2O$ (red dotted line).

Cu(II), the electronic structures, rather than the solvents employed, play an important role in the formation of products. This system with its flexible L affords delicate transition metal(II) effects in addition to strong solvent effects on the d^{10} metal cation in these self-assembly reactions.

Transesterification catalysis

Each Zn(II) catalyst (0.1 mmol) was dissolved in a mixture of methanol (10 mL) and phenyl acetate (0.13 mL, 1.0 mmol). The catalysis reactions were run at 40 °C for 10 h. The transesterification catalysis then converted phenyl acetate and methanol to phenol and methyl acetate. Their conversion yields were monitored by the corresponding ^{1}H NMR spectra (Fig. S6†). The catalysis using the 3D network, [Zn(NO$_3$)L(H$_2$O)]NO$_3$·H$_2$O, almost finished within 10 h, whereas the catalysis using the cage, [NO$_3$@Zn$_3$(NO$_3$)$_5$L$_2$]·2CH$_3$CN, had proceeded by only 14% for 10 h (Fig. 5). Thus, the two complexes show a significant difference in transesterification catalysis. Such contrasting catalytic activities can be explained by both the stability and structural differences between 3D and 0D under the catalysis conditions: that is, [NO$_3$@Zn$_3$(NO$_3$)$_5$L$_2$]·2CH$_3$CN is slowly dissociated in methanol. Thus, when a simple mixture of Zn(NO$_3$)$_2$ and L (1:1 mole ratio) was employed as a catalyst, the catalysis produced only about 17% yield for the same time. Such a fact is an interesting result that the transesterification reactions using both [NO$_3$@Zn$_3$(NO$_3$)$_5$L$_2$]·2CH$_3$CN and a simple mixture of Zn(NO$_3$)$_2$ and L (1:1 mole ratio) proceed homogeneously with dissociated catalytic species. Furthermore, when dried methanol was used in the catalysis reaction, the catalysis gave a similar pattern (Fig. S7†). However, the catalysis reaction in dried methanol was better than that in methanol including water. Such a fact is consistent with our previous results.[41]
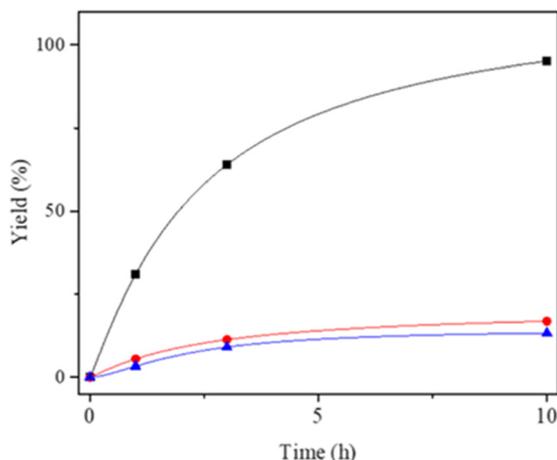
Catalysis of catechol oxidation

3,5-Di-*tert*-butylcatechol (3,5-DBCat) was employed as the substrate for the oxidation catalysis using the present copper(II) species. In particular, its oxidized form, 3,5-di-*tert*-butylquinone (3,5-DBBQ), is a potential non-innocent ligand for an intramolecular M–L electron transfer system, exhibiting a characteristic maximum absorption band at around 400 nm.[42–44] Thus, a heterogeneous catalytic oxidation reaction using [NO$_3$@Cu$_3$(NO$_3$)$_5$L$_2$(C$_2$H$_5$OH)]·C$_2$H$_5$-OH·2C$_6$H$_6$ was carried out. The catalyst was treated with 3,5-DBCat in the 1:10 mole ratio under aerobic conditions in 10 mL of acetone at 40 °C. After 3,5-DBCat and each catalyst were added to the acetone, the absorption band at 400 nm gradually increased in intensity. Thus, the relative reaction rates were monitored with reference to the increase in the UV band as a function of time (Fig. 6) along with the ^{1}H NMR spectra (Fig. S8†). The oxidation catalysis was completely finished within 180 min at room temperature. Moreover, it could be confirmed that the crystalline catalyst is more efficient than the mixture of Cu(NO$_3$)$_2$ and L. Additionally, the catalytic efficiency of the present cage crystals was compared relative to those of CuO, Cu(BF$_4$)$_2$, and Ag$_2$O.[40] The performance of the 1:100 (heterogeneous catalysts: substrate) mole catalyst has a negligible decrease, as depicted in the figure. After the reaction was completed, the mixture solution was centrifuged to recover the finely broken crystals. The IR and ^{1}H NMR spectra and PXRD patterns (Fig. S9†) indicated that the catalysts had maintained the skeletal structure after the heterogeneous catalytic reaction (Fig. S10†). The heterogeneous oxidation catalysis of the cage catalyst, [NO$_3$@Cu$_3$(NO$_3$)$_5$L$_2$(C$_2$H$_5$OH)]·C$_2$H$_5$OH·2C$_6$H$_6$, seemed to arise from the existence of the appropriate intra-cage Cu···Cu distance (4.7543(4)–5.6949(5) Å), which is suitable for the coordination with catechol.[45]

Fig. 5 Plots showing the transesterification catalysis of phenyl acetate with methanol using [Zn(NO$_3$)L(H$_2$O)](NO$_3$)·H$_2$O (black line), a mixture of Zn(NO$_3$)$_2$:L (1:1) (red line), and [NO$_3$@Zn$_3$(NO$_3$)$_5$L$_2$]·2CH$_3$CN (blue line) at 40 °C.
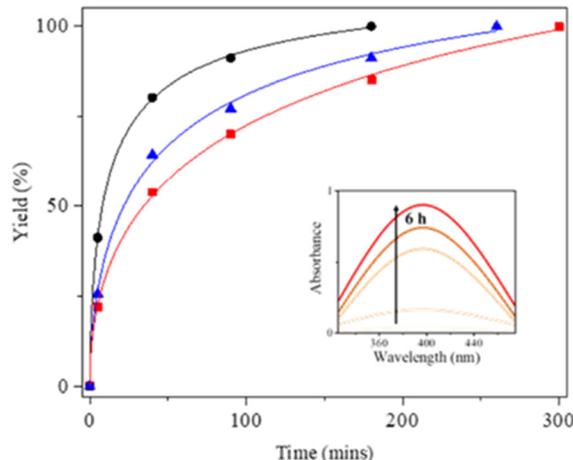
Fig. 6 Catalytic oxidation rates of 3,5-di-*tert*-butylcatechol (1 mmol) using [NO$_3$@Cu$_3$(NO$_3$)$_5$L$_2$(C$_2$H$_5$OH)]·C$_2$H$_5$OH·2C$_6$H$_6$ dependent on the catalyst quantity: 0.1 mmol (black line), 0.05 mmol (blue line), and 0.01 mmol (red line), at 40 °C in 10 mL aceton.

Conclusions

Self-assembly of the d^{10} metal cation $Zn(NO_3)_2$ with tris(2-(isoquinolin-5-yloxy)ethyl)amine (L) as a flexible tridentate ligand yields a discrete sandwich-shaped cage encapsulating a nitrate, $[Zn_3(NO_3)_6L_2]2CH_3CN$, and 3D networks, $[Zn(NO_3)L(H_2O)](NO_3)\cdot H_2O$, depending on the solvents employed. This paper provides a proof of concept that the self-assembly of a d^{10} metal(II) cation with a flexible C_3-symmetric tridentate ligand facilitates the formation of sandwich-shaped M_3L_2 architectures and 3D networks according to the polarity and shape of solvents. Further, an unusual transformation of $[NO_3@Zn_3(NO_3)_5L_2]\cdot 2CH_3CN$ into $[Zn(NO_3)L(H_2O)](NO_3)\cdot H_2O$ was observed. A similar self-assembly of $Co(NO_3)_2$ with L gave rise to 3D networks, whereas the self-assembly of $Ni(NO_3)_2$ or $Cu(NO_3)_2$ with L produced similar cages, indicating strong metal cation effects on the self-assembly. Different transesterification catalysis between the 0D cage and 3D network was observed, indicating that the structural features are key factors in catalysis. Upcoming experiments will provide more detailed information on the supramolecular ensemble's enormous potentials stemming from its catalytic–mechanistic, adsorption–desorption and photoluminescence properties.

Conflicts of interest

There are no conflicts to declare.

Acknowledgements

Notes and references

1 M. D. Allendorf, C. A. Bauer, R. Bhakta and R. Houk, *Chem. Soc. Rev.*, 2009, **38**, 1330–1352.

2 R. Chakrabarty, P. S. Mukherjee and P. J. Stang, *Chem. Rev.*, 2011, **111**, 6810–6918.

3 H. Furukawa, K. E. Cordova, M. O'Keeffe and O. M. Yaghi, *Sci.*, 2013, **341**, 1230444.

4 S. L. James, *Chem. Soc. Rev.*, 2003, **32**, 276–288.

5 C. Janiak, *Dalton Trans.*, 2003, 2781–2804.

6 S. Kitagawa, R. Kitaura and S. I. Noro, *Angew. Chem., Int. Ed.*, 2004, **43**, 2334–2375.

7 W. P. Lustig, S. Mukherjee, N. D. Rudd, A. V. Desai, J. Li and S. K. Ghosh, *Chem. Soc. Rev.*, 2017, **46**, 3242–3285.

8 B. Moulton and M. J. Zaworotko, *Chem. Rev.*, 2001, **101**, 1629–1658.

9 P. Simon and Y. Gogotsi, *Nat. Mater.*, 2008, **7**, 845–854.

10 A. V. Desai, S. Sharma, S. Let and S. K. Ghosh, *Coord. Chem. Rev.*, 2019, **395**, 146–192.

11 H. Abourahma, B. Moulton, V. Kravtsov and M. J. Zaworotko, *J. Am. Chem. Soc.*, 2002, **124**, 9990–9991.

12 J. Bernstein, R. E. Davis, L. Shimoni and N. L. Chang, *Angew. Chem., Int. Ed. Engl.*, 1995, **34**, 1555–1573.

13 S. Jeong, D. Kim and O.-S. Jung, *Cryst. Growth Des.*, 2022, **22**, 3245–3251.

14 A. Karmakar, A. Paul and A. J. Pombeiro, *CrystEngComm*, 2017, **19**, 4666–4695.

15 H. Li, M. Eddaoudi, M. O'Keeffe and O. M. Yaghi, *Nature*, 1999, **402**, 276–279.

16 H. Moon, S. W. Lim, D. Kim, O.-S. Jung and Y.-A. Lee, *CrystEngComm*, 2021, **23**, 1272–1280.

17 M. Thommes, K. Kaneko, A. V. Neimark, J. P. Olivier, F. Rodriguez-Reinoso, J. Rouquerol and K. S. Sing, *Pure Appl. Chem.*, 2015, **87**, 1051–1069.

18 D. Kim, G. Kim, J. Han and O. S. Jung, *Bull. Korean Chem. Soc.*, 2022, **43**, 1019–1031.

19 E. Barea, J. A. Navarro, J. M. Salas, N. Masciocchi, S. Galli and A. Sironi, *J. Am. Chem. Soc.*, 2004, **126**, 3014–3015.

20 L.-X. Cai, D.-N. Yan, P.-M. Cheng, J.-J. Xuan, S.-C. Li, L.-P. Zhou, C.-B. Tian and Q.-F. Sun, *J. Am. Chem. Soc.*, 2021, **143**, 2016–2024.

21 C. S. Campos-Fernández, B. L. Schottel, H. T. Chifotides, J. K. Bera, J. Bacsa, J. M. Koomen, D. H. Russell and K. R. Dunbar, *J. Am. Chem. Soc.*, 2005, **127**, 12909–12923.

22 H. Lee, J. Han, D. Kim and O.-S. Jung, *Dalton Trans.*, 2021, **50**, 14849–14854.

23 Y.-J. Zhang, T. Liu, S. Kanegawa and O. Sato, *J. Am. Chem. Soc.*, 2010, **132**, 912–913.

24 B. Manna, A. V. Desai and S. K. Ghosh, *Dalton Trans.*, 2016, **45**, 4060–4072.

25 R.-Q. Zou, J.-R. Li, Y.-B. Xie, R.-H. Zhang and X.-H. Bu, *Cryst. Growth Des.*, 2004, **4**, 79–84.

26 J. S. Jang, P. H. Borse, J. S. Lee, O.-S. Jung, C.-R. Cho, E. D. Jeong, M. G. Ha, M. S. Won and H. G. Kim, *Bull. Korean Chem. Soc.*, 2009, **30**, 1738–1742.

27 E. E. Kim and H. W. Wyckoff, *J. Mol. Biol.*, 1991, **218**, 449–464.

28 S. Lee, H. Lee and O.-S. Jung, *Dalton Trans.*, 2017, **46**, 5843–5847.

29 K. Nakashima, X. Zhou, G. Kunkel, Z. Zhang, J. M. Deng, R. R. Behringer and B. De Crombrugghe, *Cell*, 2002, **108**, 17–29.

30 M. Park, H. Kim, H. Lee, T. H. Noh and O.-S. Jung, *Cryst. Growth Des.*, 2014, **14**, 4461–4467.

31 D. R. Rosen, T. Siddique, D. Patterson, D. A. Figlewicz, P. Sapp, A. Hentati, D. Donaldson, J. Goto, J. P. O'Regan and H.-X. Deng, *Nature*, 1993, **362**, 59–62.

32 J. W. Shin, K. Eom and D. Moon, *J. Synchrotron Radiat.*, 2016, **23**, 369–373.

33 Z. Otwinowski and W. Minor, in *Methods in enzymology*, Elsevier, 1997, vol. 276, pp. 307–326.

34 G. M. Sheldrick, *SADABS, A Program for Empirical Absorption Correction of Area Detector Data*, University of Göttingen, Germany, 1996.

35 G. M. Sheldrick, *Acta Crystallogr., Sect. C: Struct. Chem.*, 2015, **71**, 3–8.

36 A. Spek, *J. Appl. Crystallogr.*, 2003, **36**, 7–13.

37 V. A. Blatov, *IUCr CompComm Newsletter*, 2006, vol. 7, p. 4.

38 B. Valeur and M. N. Berberan-Santos, *Molecular fluorescence: principles and applications*, John Wiley & Sons, 2012.

39 S.-L. Zheng, M.-L. Tong, X.-L. Yu and X.-M. Chen, *J. Chem. Soc., Dalton Trans.*, 2001, 586–592.

40 H. Irving and R. Williams, *J. Chem. Soc.*, 1953, 3192–3205.

41 E. Choi, M. Ryu, H. Lee and O.-S. Jung, *Dalton Trans.*, 2017, **46**, 4595–4601.

42 D. Kim, S. Lee, Y. A. Lee and O.-S. Jung, *Transition Met. Chem.*, 2020, **45**, 65–70.

43 J. Lee, S. Park, D. Kim, Y.-A. Lee and O.-S. Jung, *Inorg. Chem. Front.*, 2020, **7**, 1546–1552.

44 L. Yang, Y.-A. Lee and O.-S. Jung, *Inorg. Chem. Commun.*, 2019, **104**, 48–53.

45 D. Kim, G. Gwak, J. Han, D. Kim and O.-S. Jung, *Dalton Trans.*, 2022, **51**, 5810–5817.